45th AIAA/ASME/ASCE/AHS/ASC Structures, Structural Dynamics & Materials Conference
19 - 22 April 2004, Palm Springs, California

AIAA-2004-1710

Thermal Buckling of Metal Foam Sandwich Panels for Actively Cooled Thermal Protection Systems

Joseph F. Rakow * and Anthony M. Waas †

Composite Structures Laboratory,
Department of Aerospace Engineering,
University of Michigan, Ann Arbor, MI 48109-2140

March 25, 2004

Abstract

Sandwich panels with metal foam cores are studied with application to actively cooled thermal protection systems. To experimentally evaluate these panels under thermal loading, a novel technique and load frame, which provide a prominent improvement in the simultaneous preservation of thermal and mechanical boundary conditions during thermomechanical structural testing, is introduced and validated. With this technique, the response of metal foam sandwich panels (MFSP's) to thermally induced in-plane equibiaxial loading is investigated and the elasto-plastic pre- and postbuckling response of MFSP's is measured and analyzed. The in-plane response of the panels is quantified with strain gage measurements, while the out-of-plane response across the surface of the panel is captured via shadow moire interferometry. These measurements provide direct visualization and quantification of the initial buckled mode shapes as well as the evolution of the elasto-plastic post-buckled mode shapes from initial buckling into the postbuckling regime. This experimental investigation is the first of its kind, complementing the largely theoretical and numerical body of information on the thermomechanical response of sandwich panels.

*Graduate Research Assistant,

†Professor of Aerospace Engineering,
University of Michigan,
AIAA Associate Fellow,
corresponding author

1 Introduction

1.1 Current Thermal Protection Systems

Thermal protection during high speed flight is arguably the most pressing issue in the advancement of hypersonic vehicles. Since the early 1950's, with the development of the *X-2* and *X-15* vehicles, designed to capitalize on the supersonic accomplishment of the *X-1*, until last year, when the space shuttle *Columbia* disintegrated during hypersonic reentry, the technology to propel vehicles has been more mature and more successful than the technology to protect vehicles from the resulting, tremendous aerodynamic heat loads. This limitation has manifested and dominated a variety of aspects of hypersonic vehicle operation - from flight planning to vehicle maintenance to flight performance envelopes. Flight planning: the ceramic thermal protection system (TPS) on the space shuttle cannot fly in wet weather because of its hygroscopic surface. Vehicle maintenance: the shuttle TPS, as a whole, dominates the maintenance requirements of the vehicle, demanding 32,000 [1] of the 50,000 man-hours of inspection and repair required by the vehicle between flights. Performance envelopes: on its record-setting flight above Mach 6, components of the *X-15* were virtually destroyed when shock-shock interactions pierced holes in the inconel airframe, a heat sink TPS. The current state-of-the-art in TPS technology cannot efficiently manage the demanding requirements of hypersonic vehicle operation.

One concept for advanced structural thermal protection systems, and the one that promises the highest magnitude of thermal load management [2], is an actively cooled thermal protection system,

in which load bearing structural members are integrated with coolant passages. Unlike the dual-component ablative TPS onboard the manned capsules of the *Mercury*, *Gemini*, and *Apollo* aircraft and unlike the dual-component insulated system used on the space shuttle, the ideal structural thermal protection system is a single-component multifunctional structure that bears both mechanical and thermal loads.

To this point, however, true integration and multifunctionality have not been achieved. An example of a first-generation actively cooled structural panel is shown in Figure 1 [3]. This panel is a standard, honeycomb-cored sandwich panel that has been modified with a series of coolant tubes on the inside of the external face sheet. The problems associated with this type of construction are readily apparent:

1) The coolant tubes interrupt the path for shear load transfer between the face sheets and the honeycomb core

2) Machining of the honeycomb and the layup of the panel to accommodate these tubes create significant manufacturing difficulties

3) The discreet nature of the coolant passages causes severe thermal stress gradients throughout the panel

4) Blockage in discretized coolant passages leads to local hot spots of reduced strength in the load-bearing structure

For success, such problems must be overcome in next-generation actively cooled TPS concepts.

1.2 Improvements Offered by Metal Foam for Thermal Protection Systems

Metal foam sandwich panels (MFSP's) provide a truly multifunctional structure that is well-suited for the management of both thermal and mechanical loads. An actively cooled MFSP is a sandwich panel with an open-cell metal foam core integrally bonded (i.e.- brazed) to metal face sheets. While the panel bears airframe flight loads, aerodynamic heat on the panel's outer surface is conducted through the outer face sheet and, with the assistance of the conductive foam, into coolant passing through the core of the panel (Figure 2).

Metal foam is the key to the multifunctional panel, bearing mechanical shear loads while conductively distributing heat from the outer surface of the panel into and throughout the cross-sectional flow of the coolant within the panel. Metal foam, in its open cell form, has a sub-structure similar to foam found in seat cushions and packing materials, but the sub-structure is made of metallic alloy (i.e.- aluminum, titanium, inconel, copper). Figure 3 shows an open cell metal foam in detail. In previous studies, the present authors have demonstrated and characterized the response of metal foams under shear loading through experimentation [4], numerical simulation [5], and a micromechanics-based analysis [6].

Metal foam is central to the improvements offered by MFSP's over previous actively cooled panel concepts:

1) The foam and face sheets provide a monolithic, single material structure with no inherent intra-structural mismatch of coefficients of thermal expansion

2) Through-the-thickness shear response and heat transfer can be controlled through the foam density

3) The metal foam core provides a network of non-discreet coolant passages, eliminating the severity of local coolant blockage

4) With high internal surface area per unit volume ($\sim 1800\frac{m^2}{m^3}$), metal foam facilitates extremely high structure-coolant interaction in small volumes

5) In addition to conducting heat, the foam core improves the heat transfer capability of the system by creating turbulence in the coolant, even at low Reynolds numbers. The departure from laminar flow introduces a non-zero eddy coefficient, ϵ_H, into the boundary layer equations for steady, incompressible flow with constant properties, which increases the rate of heat flux, $\vec{\mathbf{Q}}$, to the coolant,

$$\vec{\mathbf{Q}} = -\rho c_p(\alpha + \epsilon_H)\frac{\partial \bar{T}}{\partial z}. \qquad (1)$$

ρ, c_p, and α are the density, specific heat at constant pressure, and thermal diffusivity of the coolant, respectively, and $\frac{\partial \bar{T}}{\partial z}$ is the time-averaged thermal gradient field perpendicular to the flow [7].

1.3 Thermomechanical Response of MFSP's

The response of MFSP's to in-plane thermomechanical loading is a driving design parameter

for the integration of MFSP's into flight-ready hardware. Previous investigations into sandwich panels and other shear deformable panels under thermal loading are almost exclusively numerical and theoretical in nature [8]–[13]; very few efforts have analyzed the thermomechanical response of sandwich panels experimentally. Likewise, no data exist, within the authors' knowledge, for the thermomechanical response of metal foam sandwich panels. Through a novel experimental technique, the present work examines the response of MFSP's under quasi-static thermally induced equibiaxial compression loads, leading to buckling and elasto-plastic postbuckling.

The first section of this paper describes the experimental procedure used in the present work to quantify the thermomechanical response of MFSP's to in-plane loading. Special attention is given to a novel experimental technique developed by the present authors to constrain and load panel-type structures without corrupting the boundary conditions in thermomechanical experiments. In common thermomechanical experimental methods, the thermal boundary conditions are corrupted by the presence of the mechanical boundary conditions, acting as a heat sink [14]. This new method represents a departure from such complications. The validity of the technique is established by measuring the onset of thermal buckling in thin monolithic aluminum plates and comparing the results to classical thin plate theory. The validated experimental technique is then utilized to subject MFSP's to thermally induced in-plane loading and to measure the response of the panels.

The next section presents the first experimental results on the thermal response and buckling of MFSP's. The in-plane response and the onset of rapid out-of-plane deflections are indicated through strain gage measurements on the panel surfaces. The measurements provide the pre- and postbuckling response of MFSP's and identify the critical temperature for the onset of thermal buckling in the panel. The out-of-plane postbuckling response, as well as the onset of thermal buckling, is captured by images of moire fringe patterns, which quantify the evolution of the elasto-plastic buckled mode shapes across the entire surface of the panel. The critical temperatures measured by both techniques are compared to a theoretical prediction based on a Rayleigh-Ritz minimization of the potential energy of a shear deformable plate. The experimental and theoretical results are shown to be in very good agreement.

2 Experimental Procedure

2.1 The Novel Load Frame

Figure 4 shows the load frame designed by the present authors to induce in-plane thermal loading of MFSP's. The central concept of the frame is to develop in-plane loads in the specimen by mismatched coefficients of thermal expansion (CTE, $\alpha(T)$). An MFSP, with a specific CTE, is clamped in a frame made of a material with a CTE that is not equal to the CTE of the MFSP material (i.e. - an aluminum MFSP in a steel frame, as is used in the present study). The frame-specimen assembly is heated uniformly[1]. Once heated, in-plane loads are created within the specimen because of the mismatched CTE's of the frame and specimen. With well-defined (measured) temperature-dependent CTE's and accurate measurements of the temperature throughout the assembly, the in-plane loading is well-defined and given by

$$\vec{\mathbf{N_T}} = \int \frac{E(z,T)\left(\alpha_{frame}(z,T) - \alpha_{panel}(z,T)\right)\Delta T(z)}{1-\nu(z,T)} dz, \tag{2}$$

in which $\vec{\mathbf{N_T}}$ is the in-plane load per unit edge length and $E = E_{panel}$ and $\nu = \nu_{panel}$.

In typical thermomechanical structural experiments, it is necessary to impart a specific temperature field or heat flux throughout the specimen. Mechanical loads must also be introduced and this typically involves contact between a load frame and the boundary of the specimen. Once contact is introduced, however, the load frame becomes a heat sink and the prescribed temperature or heat flux field in the specimen is compromised. Likewise, the severity of the thermal loading can often degrade the quality of the mechanical boundary conditions.

This challenging and occasionally prohibitive conflict is explored in [14], in which the author denotes the work of [15] as a classic example of the conflict of thermomechanical boundary conditions. The thermomechanical load frame of [15] is shown in Figure 5. In the experiment, the boundary conditions were to be clamped and one side of the panel was to be heated by radiant lamps to produce a temperature gradient through the thickness of the panel. To minimize the conductive heat sink of the clamps, the authors provided clamping along the boundary through a series of bolts. However, the

[1] Through-the-thickness thermal gradients can also be applied and are currently in use by the present authors.

bolts were not sufficient to properly realize the intended clamped boundary conditions. The insufficient clamping bolts were subsequently reinforced by stiff angle beams. The stiff angle beams, however, shaded the boundary of the panel, producing non-uniform heating of the panel. To equilibrate the in-plane temperature distribution, heat lamps were placed along the edges of the panel. However, these lamps degraded the desired thermal gradient through the thickness of the panel. The thermomechanical boundary conditions were in direct, and possibly unavoidable, conflict with each other.

The load frame designed for the present investigation offers a reprieve from the classic conflict of thermomechanical boundary conditions. The primary reason for this improvement is the fact that the boundary condition hardware is subjected to the same temperature history as the specimen. This condition eliminates thermal gradients between the specimen and load frame and allows the temperature field of the specimen to remain uncorrupted. The mechanical boundary conditions and the applied load, (2), remain well-defined throughout the experiment through measurement of the temperature-dependent material properties (CTE and moduli) of both the specimen and the frame throughout the entire temperature range of the experiment. The method has been used for both uniform and through-the-thickness static temperature fields, but remains unproven for in-plane thermal gradients and transient thermal loading.

Details of the frame are shown in Figure 6. The frame has two identical pieces that are bolted together to provide a clamped boundary condition along the border of the MFSP. This leaves a central square test section measuring $215.9x215.9mm$ $(8.5x8.5in)$. The transverse edges of the face sheets are in direct contact with the frame. Consistent, even contact along the entire perimeter of the panel is ensured with a small bead of metallic putty in the panel-frame interface. The frame has been designed such that the foam core remains accessible for both the passage of coolant and for measurements within the core. Such necessities can be accommodated because the Young's modulus of the foam core is sufficiently small to justify the assumption that the contribution of the core to the in-plane load bearing capability of the panel is negligible. The uniaxial stiffness of the foam, E_f, scales as [16]

$$E_f = (0.1 - 4.0)E_s\rho_f^2, \tag{3}$$

in which E_s is the modulus of the solid parent material and ρ_f is the relative density of the foam[2]. By substituting (3) into (2), the assumption that only the face sheets carry in-plane loads is shown to be valid for the low-density foams of interest in most sandwich structure applications.

2.2 Method Validation

To verify the accuracy of this technique, a thin square 5052-H32 aluminum plate was placed in the 1018 steel frame and subjected to a quasi-statically increasing $(1^oC/minute)$ uniform temperature field. The plate thickness is $3.175mm$ $(0.125in)$ with a $215.9x215.9mm$ $(8.5x8.5in)$ test section. Verification of the method was obtained by comparing the measured thermal buckling load with that predicted by classical thin plate theory,

$$\Delta T_{cr} = \left(\frac{4\pi^2}{9}\right)\left(\frac{1}{(\alpha_{frame} - \alpha_{panel})(1+\nu)}\right)\left(\frac{t}{a}\right)^2, \tag{4}$$

in which ΔT_{cr} is the temperature at bifurcation and $\frac{t}{a}$ is the ratio of plate thickness to edge length.

Figure 7 shows the strain versus temperature history of one of the plate specimens measured by back-to-back strain gage pairs and the comparison of the measured bifurcation point with that predicted by (4). The precise bifurcation point was determined with a southwell plot [17] and strain decomposition, as are used and explained in the following section for MFSP's. The data indicates agreement between theory and experiment to within 5%, which verifies that this experimental technique induces in-plane loading and bifurcation in the fashion predicted by (4). A second monolithic aluminum plate was tested to establish repeatability in the verification of this technique. The experimentally measured critical buckling temperatures of the two plates are listed in Table 1, along with the theoretical prediction from (4).

2.3 MFSP Specimens and Instrumentation

The aluminum foam sandwich panels analyzed in the present work are shown in Figure 8. The panels measure $254x254mm$ $(10x10in)$. The core has a thickness of $6.35mm$ $(0.25in)$. The foam is made from 6101-T6 aluminum and has 8 pores per centimeter (20 pores per inch) and a relative

[2]Relative density of foams is defined as the density of the foam divided by the density of the parent material from which it is foamed, expressed as a percentage.

density of $\rho_f = 8\%$. The core is brazed to 6061-T6 aluminum face sheets, which have a thickness of $1mm$ $(0.04in)$. The panels were manufactured by ERG Materials and Aerospace Corporation (Oakland, CA). Four identical specimens were subjected to uniform thermal loading and unloading in the steel frame.

An instrumented panel-frame setup is illustrated in Figure 9. Each of the specimens was instrumented with five distributed type-K Nextel-insulated thermocouples (XC-20-K-72, Omega Engineering) with electronic ice point reference junctions. The locations of the five thermocouples varied among the tests and were chosen from the locations shown in Figure 9. The purpose of the range of locations was to ensure that the panel-frame assembly experienced no thermal gradients, in the plane of the panel or through the thickness of the assembly. Each combination of thermocouple locations confirmed a uniform temperature field throughout the entire assembly over the duration of the experiment, as can be seen by the thermal loading curve in Figure 10.

Two of the specimens were instrumented with high-temperature, fully encapsulated Karma-based alloy strain gages (WK-062AP-13-350, Vishay Micromeasurements), arranged in back-to-back pairs located in the center of each face sheet of the panel, parallel and perpendicular to the boundary of the test section. Multiple co-axial strain gages were used for redundancy in the measurement system. The appendix to the present paper describes the procedure for post-processing of the raw strain gage measurements, accounting for thermal effects on the strain gage material.

The other two specimens were instrumented for shadow moire interferometry [18], measuring the out-of-plane displacement field as the panel buckled and deformed into the postbuckling regime. In the shadow moire method, as illustrated in Figure 11, a specimen is put in contact with a ronchi ruling, which is a glass substrate marked with parallel black lines evenly spaced at a pitch, p. A white light source shines through the ruling onto the specimen at a non-zero angle, β, with respect to the normal axis of the specimen. The light reflects off of the surface of the specimen, passes back through the ruling, and produces an interference pattern that is captured by a digital camera also oriented at a non-zero angle, γ. The interference pattern is a contour representation of out-of-plane displacements. Each fringe represents a differential displacement magnitude, Δw, such that

$$\Delta w = \frac{p}{\cos\beta + \cos\gamma}. \tag{5}$$

In the present experiments, the light source and camera are oriented at angles of $\beta = 8.5^o$ and $\gamma = 9.7^o$, respectively, from the normal axis of the panel. With a pitch of $12lines/mm$ $(300lines/in)$ on the glass substrate, the increment of out-of-plane deflection represented by each fringe is $\Delta w = 0.264mm$ $(.0104in)$.

With an average temperature defined by the thermocouple measurements, the local bending and membrane strains measured by the strain gages and the full out-of-plane displacement field measured by the moire fringe patterns provide a temperature-based history of the thermally induced pre-buckling, buckling, and postbuckling response of MFSP's.

2.4 Thermal Loading

The panel-frame assembly was subjected to uniform thermal loading in an oven. The temperature-time history is a simple load-unload quasi-static cycle with a temperature rise rate of $1^oC/minute$, a peak temperature of 300^oC, and an uncontrolled free convection cool-down to room temperature. The peak temperature was dictated by the maximum temperature of the oven. This load cycle is shown in Figure 10. The figure shows the temperature measurement of five thermocouples distributed across both sides of the panel-frame assembly. Thermal gradients are shown to be minimal or non-existent throughout the duration of the experiment.

3 Results and Discussion

3.1 In-plane Response

The response of MFSP's to uniform thermal loading and unloading is shown in Figure 12. As the temperature rises, equibiaxial tensile strains develop equivalently on each side of the panel. From points A to B in the figure, the panel is in the pre-buckled state. The tensile aggregate strain state is accompanied by a compressive aggregate stress state. This is possible because a non-zero temperature change, $\Delta T \neq 0$, is introduced into the thermoelastic constitutive relations,

$$\sigma_{\mathbf{ij}} = \lambda\delta_{\mathbf{ij}}\epsilon_{\mathbf{kk}} + 2G\epsilon_{\mathbf{ij}} - (3\lambda + 2G)\delta_{\mathbf{ij}}\alpha\Delta T. \tag{6}$$

The tensile aggregate strains have a positive thermal strain component and a negative mechanical strain component, due to the constricting frame, which result in compressive stresses in the panel. The magnitudes and signs of the thermal and mechanical strain components during the load-unload thermal cycle will be discussed in further detail at the end of this section.

At point B, the panel buckles and the strain states on opposite sides of the panel diverge and continue diverging until the peak temperature at point C. The strain response at and around the point of buckling is shown in Figure 13. The panel buckles symmetrically in both the x- and y-directions and the shape can be represented by

$$w(x,y) = \sin\left(\frac{\pi x}{a}\right)\sin\left(\frac{\pi y}{a}\right)\cdots \sum_{m=1}^{\infty}\sum_{n=1}^{\infty} A_{mn}\sin\left(\frac{m\pi x}{a}\right)\sin\left(\frac{n\pi y}{a}\right), \quad (7)$$

in which $w(x,y)$ is the magnitude of out-of-plane deflection. (7) is the series of mode shapes used in the Rayleigh-Ritz analysis, which will be formulated in a later subsection of the present paper.

Beyond buckling, between points B and C, it is clear from Figure 12 that the aggregate strain on the front side of the panel becomes increasingly compressive relative to the aggregate strain on the back side of the panel. This behavior continues until the peak temperature at point C. From points C to D, the temperature decreases through free convection, releasing all elastic thermal and mechanical strain components. Once unloaded, the accumulated plastic strain in the panel is shown at point D. A detailed analysis of the thermoelastic-plastic strain components is given later in this section.

A critical design criterion for in-plane loads in thermal protection systems such as actively cooled MFSP's is the buckling point. Although a buckling point is identifiable in Figure 13, a more accurate numerical value may be obtained by transforming the strain-temperature measurements into two different forms. The first is a decomposition of the strain into bending and membrane modes as is shown in Figure 14. From this plot, it is clear that the panel is in a state of pure membrane deformation until a clear, distinct onset of bending deformation, indicating buckling within the panel.

The second useful transformation of data is a temperature-based southwell plot for plate buckling [17]. A typical southwell plot, for mechanical buckling of columns, is obtained by considering

$$w = P_{cr}\frac{w}{P} - w_o \quad (8)$$

and plotting $\frac{w}{P}$ versus w. w is the lateral deflection of the midpoint of the column, w_o is the amplitude of initial curvature in the imperfect column, and P is the end load. The inverse slope of the southwell plot is the buckling load of the column. The analog to this procedure for thermal buckling in panels is represented by

$$\epsilon_b = \frac{\Delta T_{cr}}{\Delta T}\epsilon_b - w_{o,xx} \quad (9)$$

and the inverse slope of a plot of $\frac{\epsilon_b}{\Delta T}$ versus ϵ_b yields the buckling temperature, ΔT_{cr}, of the panel. Such a plot is shown in Figure 15.

Both the strain decomposition technique and the southwell method are used to identify the buckling point of the two panels instrumented with strain gages. The buckling temperatures, ΔT_{cr}, of the four MFSP specimens are shown in Table 2 with a comparison to a theoretical prediction. The results show repeatability of the measurements and close correlation to theory. The theoretical development is discussed in a later subsection of the present paper. The results from experiments with the two MFSP's instrumented for moire interferometry are explained in detail in the following section.

The temperature history of the thermal and mechanical elastic and plastic strain components, throughout the duration of the loading cycle, are shown in Figure 16. The aggregate strain state is decomposed into its thermal and mechanical (elastic and plastic) components. This is possible because $\alpha(T)$ and $\Delta T(t)$ are known for the MFSP's.

Throughout the duration of the experiment, point A through point D, the thermal strain is positive in the panel, as is dictated by $\Delta T \geq 0$. The magnitude of thermal strain dominates the aggregate strain state throughout the loading cycle and most of the unloading cycle of the experiment. From point A to point B to point C, the mechanical strain state follows qualitatively similar behavior as the aggregate strain analysis described in detail above and in Figure 12 and Figure 13. The mechanical strains are similar on both sides of the panel until buckling, at which point the strains diverge until the peak temperature is reached at point C.

From point C to point D in Figure 16, interesting elasto-plastic behavior is shown that could not be revealed by the aggregate strain analysis. Thermal unloading initially produces a decrease in

mechanical strain (elastic strain) of approximately 22% of the peak mechanical strain on each side of the panel. After this initial relaxation, the mechanical strain reaches a plateau for the remainder of the thermal unloading. Although elastic mechanical strain is released, the bending strain, the difference between the mechanical strains on each side of the panel, remains constant for the entire unloading cycle. This is readily apparent in Figure 16. The release of elastic strain, then, is exclusively membrane strain, attributed to the loss of in-plane loading from the constricting frame. The curvature that was present in the panel at the peak temperature (point C) is wholly present when the panel is completely unloaded (point D). This behavior will be visualized with shadow moire interferometry in the next section.

3.2 Out-of-plane Response

An analysis by shadow moire interferometry is used to identify the critical temperatures, the buckling mode shapes, and the postbuckling response of the MFSP's. In-situ images of the MFSP's under thermal loading were captured throughout the response experiment. Figure 17 shows the moire fringe patterns captured at each of the lettered response points in Figure 12. At point A, there is a slight fringe pattern, which indicates the level of imperfection in the measurement system - initial panel curvature, misalignment of the ronchi ruling, or curvature in the ruling. This image serves as a reference state for the analysis. The image at point A remains unchanged until point B because there is no appreciable relative out-of-plane deformation in the pre-buckling regime.

At point B, the first sign of thermomechanical out-of-plane curvature appears as a black spot at the center of the panel, which is indicated by the white arrow in Figure 17. This occurs at the same temperature that the strain gage measurements begin to diverge in Figure 12 and Figure 13. The appearance of the black spot in the center of the panel indicates the first critical temperature of the MFSP's. From point B to point C, the fringe pattern evolves as the panel continues to deflect out of the plane of loading with a new fringe appearing and growing from the center of the panel each time the center of the panel deflects $\Delta w = 0.264mm$ $(.0104in)$.

At point C, the panel is fully loaded ($T = 300^oC$) and a clear set of fringes provide a precise measurement of the out-of-plane deflection over the entire surface of the panel. After point C, the panel is unloaded and all elastic deformation is released.

At point D, when the panel is fully unloaded, the fringe pattern has not changed appreciably from point C. This indicates that only a small amount of the out-of-plane deflection is elastic for the geometry and thermal loading used in the present investigation. The images between points C and D confirm the findings of the elasto-plastic strain analysis of the previous section. Thermal unloading of these MFSP's released membrane strain, while the bending strain proved to be plastic.

It would be informative to obtain measurements of MFSP's further into the postbuckling regime than those presented in Figure 17. However, the peak temperature of the oven prohibits the investigation of the postbuckling response of MFSP's at higher temperatures. To further investigate the postbuckling response of MFSP's without requiring higher test temperatures, an imperfection was introduced into a fifth MFSP specimen to induce relatively large out-of-plane deflections early in the thermal loading history and to allow imaging of the postbuckling mode shapes across a larger portion of the postbuckling regime.

To introduce the imperfection into the MFSP, the clamping bolts on the frame were over-tightened such that the edges of the entire perimeter of the panel were forced to curve towards each other, into the core, creating an initial curvature in each face of the panel. The imperfect panel was then subjected to the same thermal loading that the perfect panels experienced and images were captured of the moire fringe patterns. Figure 18 shows the postbuckling mode shapes of the MFSP as the temperature rises above the critical temperature of the imperfect panel.

The images of the fringe patterns are quantified into data that highlights the thermal postbuckling behavior of MFSP's. Figure 19 shows the magnitude of out-of-plane deflection of the center point of the panel versus normalized temperature, $\frac{\Delta T}{\Delta T_{cr}}$. The onset of buckling is followed by a rapid increase in out-of-plane deflection. This initial buckling behavior relaxes into a steady postbuckling response.

The evolution of the mode shapes throughout postbuckling is further illustrated by considering the deflection of a line on the panel's surface as the temperature increases beyond bifurcation. Figure 20 shows the out-of-plane deflection at postbuckling temperatures of a line lying along the x-axis of the specimen, as quantified through the moire fringe patterns. Due to symmetry, the response of the material along the x-axis is equivalent to that of mate-

rial along the y-axis. It is clear from this figure that the center portion (i.e.- the middle $40mm$) of the panel remains relatively flat throughout the post-buckling response, while deformation accumulates in the lobes of the curvature in the form of increasing slope.

This finding adds further insight to the strain analysis discussed in the previous section. The strain gages, as shown in Figure 9, are located at $x = 0mm$ in Figure 20. The bending strain measured by the gages at the center of the panel, shown in Figure 14, then is a representation of curvature at $x = 0$. At the onset of buckling, the maximum bending strain is shown to be at $x = 0$. As the mode shapes evolve, however, Figure 20 shows that the maximum bending strain and stress is no longer in the center of the panel. This can be seen in Figure 18 as well. The density of the contours shifts from the center of the MFSP during initial buckling towards the boundary of the panel in the postbuckling regime.

3.3 Comparison with Theory

The energy formulation for the thermal loading of a sandwich panel, as developed in [8] and [9], is presented and adapted to the problem at hand. The formulation considers a rectangular sandwich panel under thermal loading due to a static uniform temperature change. The sandwich panel is considered to be a shear-deformable plate, such that there is no account of the cross-sectional kinematics of a sandwich panel, specifically. The rotation of a cross-sectional normal is represented by a single variable, akin to a Reissner-Mindlin formulation. The geometry and material properties of the panel core determine the constitutive properties of the plate under shear loading while the geometry and material properties of the face sheets determine the constitutive properties of the plate under in-plane loads and bending moments. Using standard notation for laminated plate theory [19], the constitutive relations for the sandwich panel are taken to be

$$\begin{bmatrix} N_x \\ N_y \\ N_{xy} \end{bmatrix} = \begin{bmatrix} A_{11} & A_{12} & 0 \\ A_{21} & A_{22} & 0 \\ 0 & 0 & A_{66} \end{bmatrix} \begin{bmatrix} \frac{\partial u}{\partial x} \\ \frac{\partial v}{\partial y} \\ \frac{\partial u}{\partial y} + \frac{\partial v}{\partial x} \end{bmatrix} - \begin{bmatrix} N_x^T \\ N_y^T \\ N_{xy}^T \end{bmatrix},$$

$$\begin{bmatrix} M_x \\ M_y \\ M_{xy} \end{bmatrix} = \begin{bmatrix} D_{11} & D_{12} & 0 \\ D_{21} & D_{22} & 0 \\ 0 & 0 & D_{66} \end{bmatrix} \cdots \begin{bmatrix} -\frac{\partial}{\partial x}\left(\frac{\partial w}{\partial x} - \gamma_{xz}\right) \\ -\frac{\partial}{\partial y}\left(\frac{\partial w}{\partial y} - \gamma_{yz}\right) \\ -\frac{\partial}{\partial y}\left(\frac{\partial w}{\partial x} - \gamma_{xz}\right) - \frac{\partial}{\partial x}\left(\frac{\partial w}{\partial y} - \gamma_{yz}\right) \end{bmatrix} - \begin{bmatrix} M_x^T \\ M_y^T \\ M_{xy}^T \end{bmatrix},$$

in which

$$\begin{bmatrix} N_x^T & , & M_x^T \\ N_y^T & , & M_y^T \\ N_{xy}^T & , & M_{xy}^T \end{bmatrix} = \sum_{i=1}^{2} \left[t_s T_i, (-1)^i \frac{t_s h}{2} T_i \right] \cdots \begin{bmatrix} \frac{E}{1-\nu^2} & \frac{E\nu}{1-\nu^2} & 0 \\ \frac{E\nu}{1-\nu^2} & \frac{E}{1-\nu^2} & 0 \\ 0 & 0 & G_{xy} \end{bmatrix}_i \begin{bmatrix} \alpha_x \\ \alpha_y \\ \alpha_{xy} \end{bmatrix}_i,$$

and

$$\begin{bmatrix} Q_x \\ Qy \end{bmatrix} = \begin{bmatrix} D_{Q_x} & 0 \\ 0 & D_{Q_y} \end{bmatrix} \begin{bmatrix} \gamma_{xz} \\ \gamma_{yz} \end{bmatrix}. \tag{10}$$

The boundary conditions are such that the panel boundary cannot displace in the plane of the panel and, in the case considered in the present work, all edges are clamped. Accordingly,

$$w(x,y) = \sin\left(\frac{\pi x}{a}\right) \sin\left(\frac{\pi y}{b}\right) \cdots \sum_{m=1}^{\infty} \sum_{n=1}^{\infty} A_{mn} \sin\left(\frac{m\pi x}{a}\right) \sin\left(\frac{n\pi y}{b}\right)$$

$$\gamma_{xz} = \cos\left(\frac{\pi x}{a}\right) \sin\left(\frac{\pi y}{b}\right) \cdots \sum_{m=1}^{\infty} \sum_{n=1}^{\infty} B_{mn} \sin\left(\frac{m\pi x}{a}\right) \sin\left(\frac{n\pi y}{b}\right) + + \sin\left(\frac{\pi x}{a}\right) \sin\left(\frac{\pi y}{b}\right) \cdots \sum_{m=1}^{\infty} \sum_{n=1}^{\infty} m B_{mn} \cos\left(\frac{m\pi x}{a}\right) \sin\left(\frac{n\pi y}{b}\right)$$

$$\gamma_{yz} = \sin\left(\frac{\pi x}{a}\right) \cos\left(\frac{\pi y}{b}\right) \cdots \sum_{m=1}^{\infty} \sum_{n=1}^{\infty} C_{mn} \sin\left(\frac{m\pi x}{a}\right) \sin\left(\frac{n\pi y}{b}\right) +$$

$$+ \sin\left(\frac{\pi x}{a}\right)\sin\left(\frac{\pi y}{b}\right)\cdots$$
$$\sum_{m=1}^{\infty}\sum_{n=1}^{\infty} nC_{mn}\sin\left(\frac{m\pi x}{a}\right)\cos\left(\frac{n\pi y}{b}\right).$$

The potential energy of the heated panel is minimized with respect to each of the degrees of freedom, such that

$$\frac{\partial \Pi}{\partial A_{mn}} = \frac{\partial \Pi}{\partial B_{mn}} = \frac{\partial \Pi}{\partial C_{mn}} = 0 \qquad (11)$$

produces three equations for each $mnkl$, relating A_{mn}, B_{mn}, C_{mn},

$$\sum_{k}^{\infty}\sum_{l}^{\infty}\left\{\left[a^{11}_{mnkl} + \eta\frac{D^{\star}}{ab}\left(\frac{\pi}{a}\right)^2 k_{xy}\delta_{mnkl}\right]A_{kl} + \right.$$
$$\left. + a^{12}_{mnkl}B_{kl} + a^{13}_{mnkl}C_{kl}\right\} = 0 \qquad (12)$$
$$\sum_{k}^{\infty}\sum_{l}^{\infty}\left[a^{21}_{mnkl}A_{kl} + a^{22}_{mnkl}B_{kl} + a^{23}_{mnkl}C_{kl}\right] = 0$$
$$\sum_{k}^{\infty}\sum_{l}^{\infty}\left[a^{31}_{mnkl}A_{kl} + a^{32}_{mnkl}B_{kl} + a^{33}_{mnkl}C_{kl}\right] = 0.$$

Solution of (12) leads to a thermal buckling criterion of the form

$$\sum_{k}\sum_{l}\left[\frac{M_{mnkl}}{\Delta T} + P_{mnkl} + \delta_{mnkl}\right]A_{kl} = 0, \qquad (13)$$

in which M_{mnkl} is the bending stiffness parameter, P_{mnkl} is the extensional stiffness parameter, and δ_{mnkl} is a delta function dependent on the mechanical boundary conditions of the system. The buckling criterion can be evaluated with temperature-dependent material properties in an iterative process. For further details of the derivation, the reader is referred to [8] and [9].

This formulation provides a prediction of the critical temperature of the MFSP's studied in the present work. When evaluated for a square panel with clamped boundary conditions, the theoretical prediction is shown in Table 2 to be very similar to the experimentally measured values for the onset of buckling.

The theory, in its original form, cannot be used to model the pre- or postbuckling response measured in the present investigation for two reasons. First, the theory assumes rigid in-plane boundary conditions and, therefore, a null strain state in the pre-buckling regime. To model the pre-buckling behavior measured in the experiments, the analysis would require elastic in-plane boundary conditions. Second, the theory is a linear strain theory and, therefore, cannot predict a postbuckling response. A non-linear extension of this theory and the inclusion of elastic in-plane boundary conditions, accompanied by a comparison with the pre- and postbuckling response measured in the present experiments, is the subject of ongoing research by the present authors.

4 Conclusion

The response of MFSP's to thermally induced equibiaxial in-plane loading has been investigated experimentally. Within the authors' knowledge, these are the first successful experimental measurements of the response of sandwich panels to thermally induced in-plane loads. The results are intended to complement the relatively extensive theoretical and numerical investigations on the subject matter. Measurements have been made of the elastoplastic in-plane and out-of-plane response of MFSP's in the pre- and postbuckling regimes. The first critical buckling temperature has been measured and compared favorably to existing theory. The onset and evolution of the buckled mode shapes have been measured through shadow moire interferometry. The images, coupled with strain gage measurements, provide a useful illustration of the in-plane and out-of-plane response of MFSP's to thermal loading up to and beyond critical design parameters. The experimental results have been obtained with a novel technique, designed to circumvent the problems commonly encountered with experimental thermomechanical boundary conditions. A comparison of experimental results for a solid thin aluminum plate to classical thin plate buckling theory provided validation of the thermal loading technique. An understanding of the thermal buckling behavior of MFSP's is critical to the development of these panels for actively cooled thermal protection systems. The experiments presented in the present paper provide a foundation for the experiments on actively cooled inconel foam sandwich panels currently under investigation by the present authors.

Acknowledgements

This research has been financially supported by NASA URETI award NCC 3989 through NASA Marshall and Glenn Research Centers.

References

[1] S.J. Scotti. Thermal protection systems for reusable launch vehicles. *Symposium on Structures for Hypersonic Vehicles, ASME International Congress*, November 2003.

[2] H.N. Kelly and M.L. Blosser. Active cooling from the sixties to NASP. *Current Technology for Thermal Protection Systems*, NASA CP-3157:189–249, 1992.

[3] D.A. Ellis, L.L. Pagel, and D.M. Schaeffer. Design and fabrication of a radiative actively cooled honeycomb sandwich structural panel for hypersonic aircraft. NASA CR-2957, 1978.

[4] J.F. Rakow and A.M. Waas. Size effects and the shear response of aluminum foam. *Mechanics of Materials*, 2004. Available at www.sciencedirect.com under "Articles in Press".

[5] J.F. Rakow and A.M. Waas. Size effects in metal foam cores for sandwich structures. *AIAA Journal*, May 2004.

[6] J.F. Rakow and A.M. Waas. The effective isotropic moduli of random fibrous composites, platelet composites, and foamed solids. *Mechanics of Advanced Materials and Structures*, 11(2):151–173, 2004.

[7] F.P. Incropera and D.P. DeWitt. *Fundamentals of Heat and Mass Transfer*. John Wiley and Sons, New York, NY, fifth edition, 2002.

[8] W.L. Ko. Mechanical and thermal buckling analysis of sandwich panels under different edge conditions. NASA TM-4535, 1993.

[9] W.L. Ko. Predictions of thermal buckling strengths of hypersonic aircraft sandwich panels using minimum potential energy and finite element methods. NASA TM-4643, May 1995.

[10] A.K. Noor and J.M. Peters. Postbuckling of multilayered composite plates subjected to combined axial and thermal loads. In E.A. Thornton, editor, *Thermal Structures and Materials for High-Speed Flight*, volume 140, pages 183–203, 1992.

[11] T. Hause, L. Librescu, and T.F. Johnson. Nonlinear response of geometrically imperfect sandwich curved panels under thermomechanical loading. *International Journal of Non-Linear Mechanics*, 33(6):1039–1059, 1998.

[12] R. Javaheri and M.R. Eslami. Thermal buckling of functionally graded plates based on higher order theory. *Journal of Thermal Stresses*, 25:603–625, 2002.

[13] H.S. Shen. Thermomechanical post-buckling analysis of imperfect laminated plates using a higher-order shear-deformation theory. *Computers and Structures*, 66(4):395–409, 1998.

[14] M.L. Blosser. Boundary conditions for aerospace thermal-structural tests. *Progress in Aeronautics and Astronautics*, 168:119–144, 1995.

[15] W.L. Richards and R.C. Thompson. Titanium honeycomb panel testing. NASA TM-4768, 1996.

[16] M.F. Ashby et al. *Metal Foam: A Design Guide*. Butterworth-Heinemann, Boston, MA, 2000.

[17] J. Singer et al. *Buckling Experiments: Experimental Methods in Buckling of Thin-walled Structures, volume 1*. John Wiley and Sons, New York, NY, 2002.

[18] P.S. Theocaris. *Moire Fringes in Strain Analysis*. Pergamon Press, New York, NY, 1969.

[19] J.N. Reddy. *Mechanics of Laminated Composite Plates*. CRC Press, New York, NY, 1997.

Appendix

The strains shown in Figure 12 and Figure 13 are not raw strain measurements obtained by measuring the change in gage resistance with increased loading, as would be done in a room temperature strain analysis. Raw strain gage measurements at elevated temperature are in error from two sources: 1) the temperature dependence of the gage factor, $k(T)$, 2) the apparent strain caused by differential free thermal expansion between the test specimen and the gage itself.

If a test panel were instrumented with a strain gage, heated, and allowed to expand freely, the strain gage would read an apparent strain, ϵ_{app}^{free},

$$\epsilon_{app}^{free} = \frac{k}{k(T)}[\frac{\gamma \Delta T}{k} + (\epsilon_{panel}^{free} - \epsilon_{gage})], \qquad (14)$$

in which k is the gage factor at room temperature, $k(T)$ is the gage factor at elevated temperatures, γ is the thermal coefficient of resistance of the gage alloy, ϵ_{panel}^{free} is the actual strain in the freely expanded panel, and ϵ_{gage} is the strain in the gage due to thermal expansion of the gage itself.

Similarly, if the instrumented panel were heated while constrained in the steel frame, the strain gage would read an apparent strain for the constrained panel at each temperature, ϵ_{app}^{con},

$$\epsilon_{app}^{con} = \frac{k}{k(T)}[\frac{\gamma \Delta T}{k} + (\epsilon_{panel}^{actual} - \epsilon_{gage})]. \qquad (15)$$

$\epsilon_{panel}^{actual}$ is the actual strain in the constrained panel and ϵ_{gage} is the strain in the gage due to thermal expansion of the gage itself.

In subtracting (14) from (15) and assuming strain gages from the same manufacturer's lot are used in each test, which is the case in the present investigation, the strain associated with thermal stresses, ϵ_{stress}, is recovered,

$$\epsilon_{stress} = \frac{k}{k(T)}[\epsilon_{panel}^{actual} - \epsilon_{panel}^{free}], \qquad (16)$$

and can be solved for $\epsilon_{panel}^{actual}$. Before solving (16), the temperature-dependent magnitude of ϵ_{panel}^{free} is found by measuring the free thermal expansion of the panel with respect to a reference material made of titanium-silicate, which has a negligible coefficient of thermal expansion over the range of temperatures investigated in the present work. This procedure produces accurate measurements of $\epsilon_{panel}^{actual}$, the actual strain that the panel experiences when constrained in the frame and heated. $\epsilon_{panel}^{actual}$ is the quantity plotted in Figure 12 and Figure 13.

	ΔT_{cr}(C)	Difference
Theory	62	-
Plate1	63	1.6%
Plate2	59	4.8%

Table 1: Critical temperatures of thin monolithic 5052-H32 aluminum plates

	ΔT_{cr}(C)	Difference	Measurement Method
Theory	167	-	-
Panel1	188	12.6%	Strain Gages
Panel2	175	4.8%	Strain Gages
Panel3	170	1.8%	Moire Fringes
Panel4	176	5.4%	Moire Fringes

Table 2: Critical temperatures of aluminum foam sandwich panels

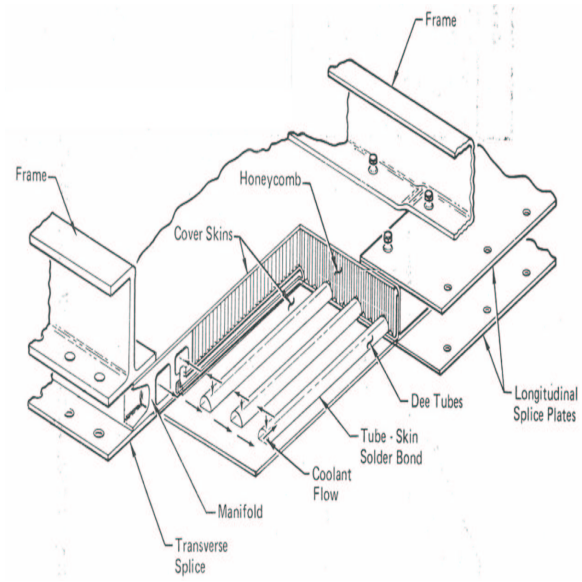

Figure 1: A first-generation actively cooled sandwich panel [3]

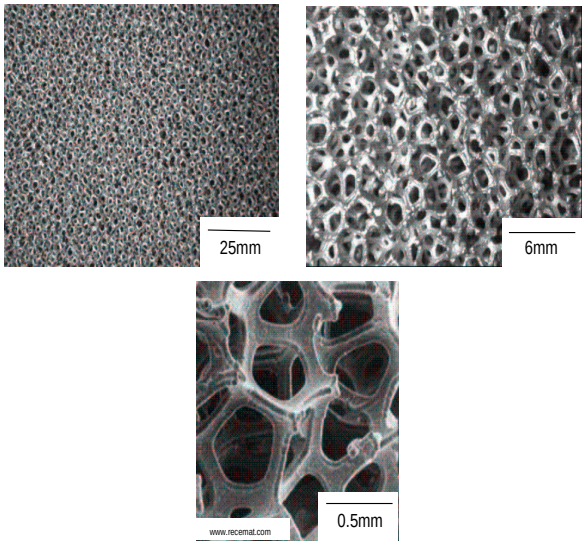

Figure 3: Open cell metal foam

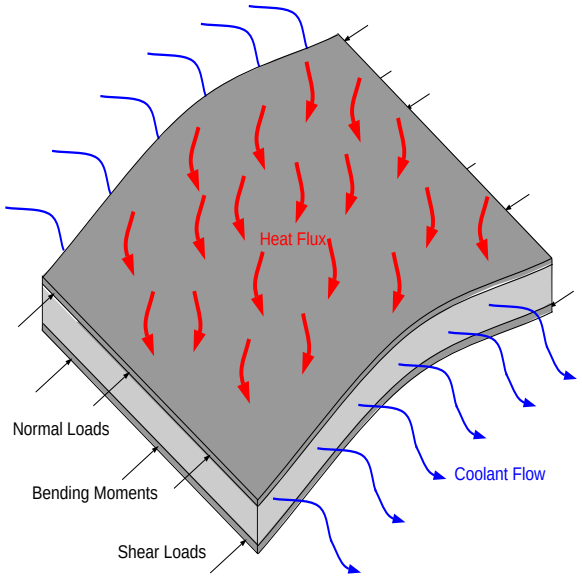

Figure 2: Schematic of an actively cooled MFSP

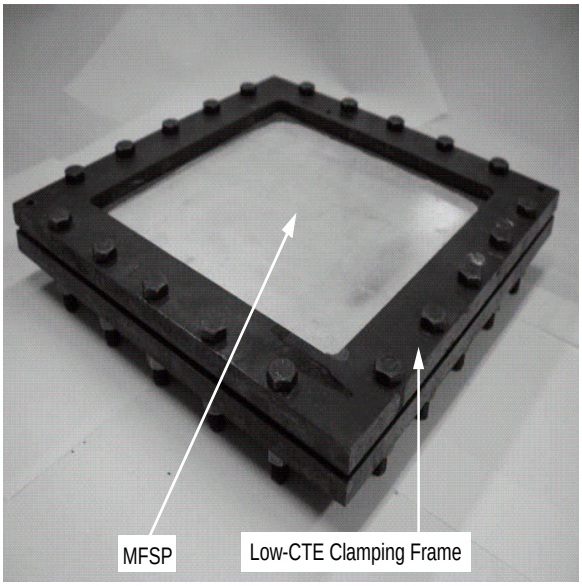

Figure 4: The load-frame used to clamp the boundary of the MFSP and to induce in-plane thermal stresses

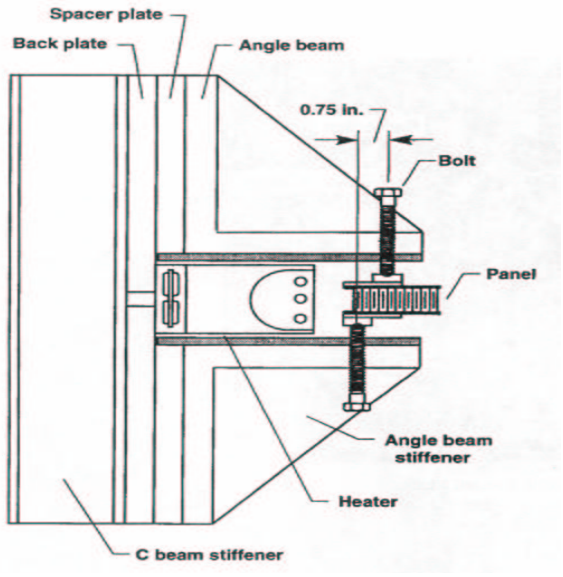

Figure 5: A thermal structural load frame that demonstrates the conflicts typical of experimental thermomechanical boundary conditions

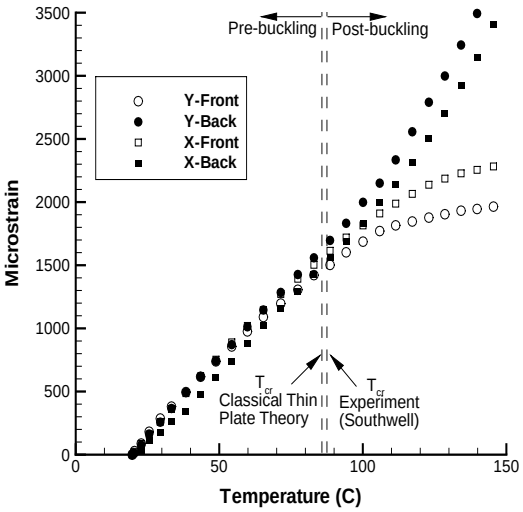

Figure 7: The response of a thin plate to thermal loading demonstrates the validity of the experimental technique

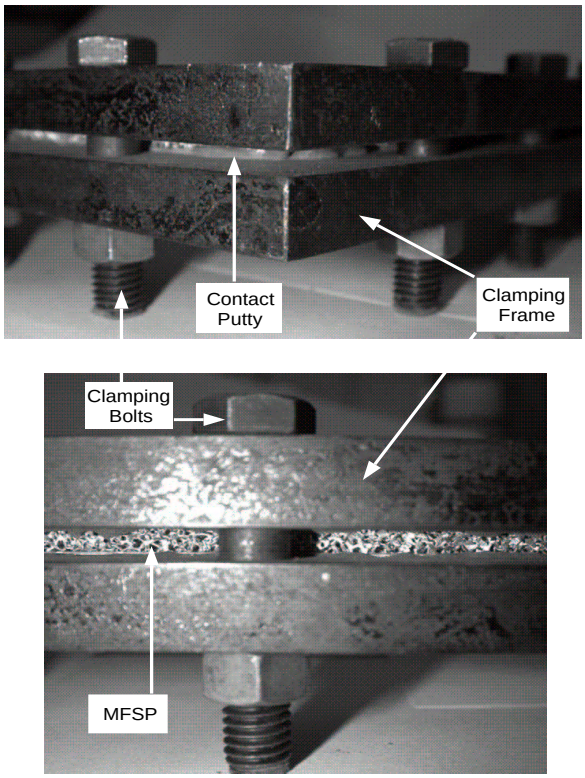

Figure 6: Details of the steel load frame

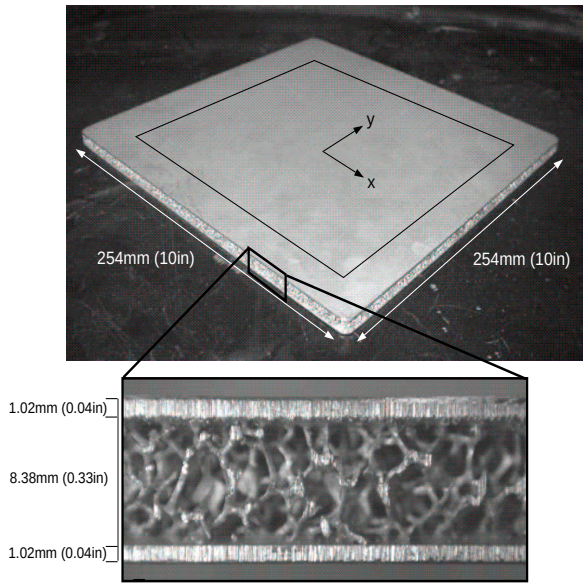

Figure 8: The MFSP's used to obtain the results of the present work

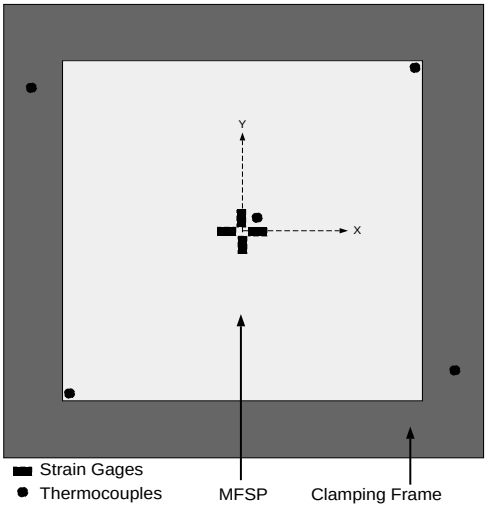

Figure 9: Location of the strain gages and thermocouples on the instrumented panel-frame setup. The instrument locations are identical on each side of the assembly.

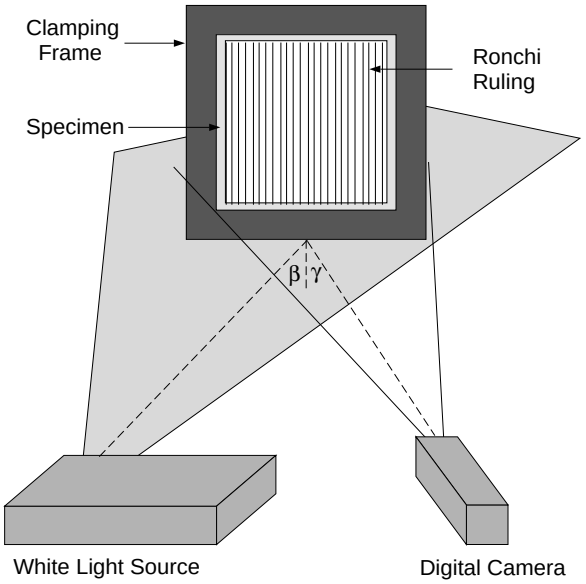

Figure 11: The setup for measuring buckling modes with shadow moire interferometry

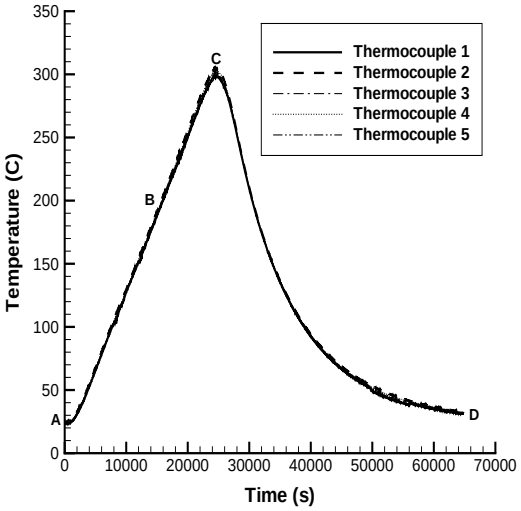

Figure 10: Five simultaneous thermocouple readings demonstrate the uniformity of the applied temperature in the experiments

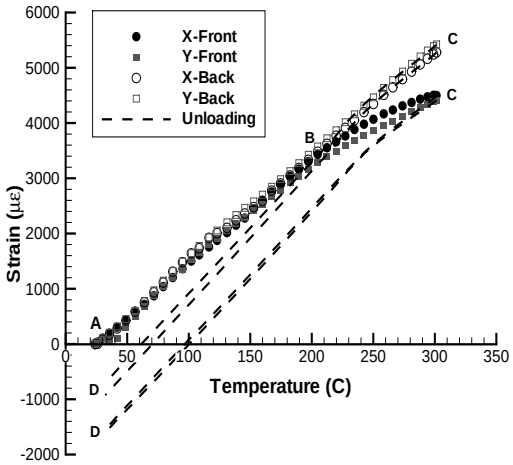

Figure 12: The response of MFSP's to thermal loading and unloading

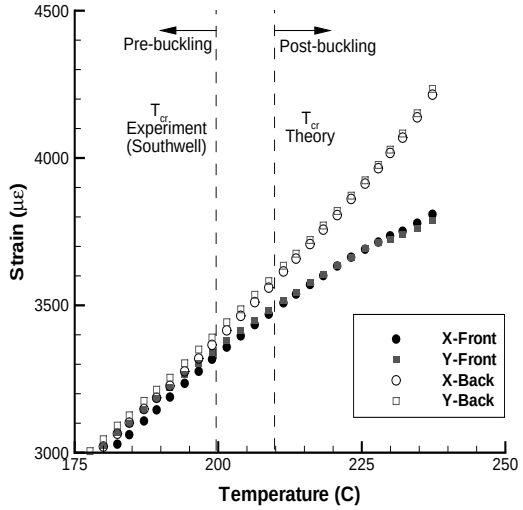

Figure 13: The response of MFSP's to thermal loading at the point of thermal buckling

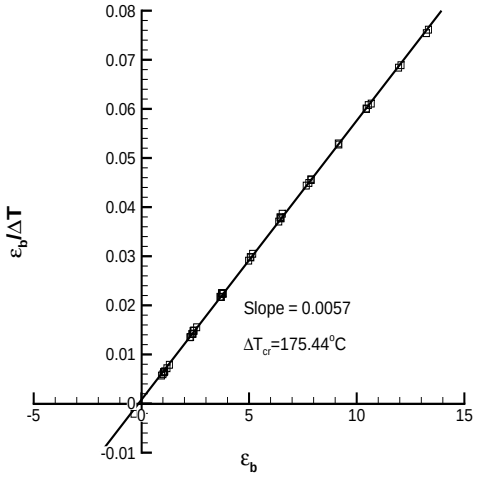

Figure 15: A southwell plot determines the buckling temperature of the MFSP's

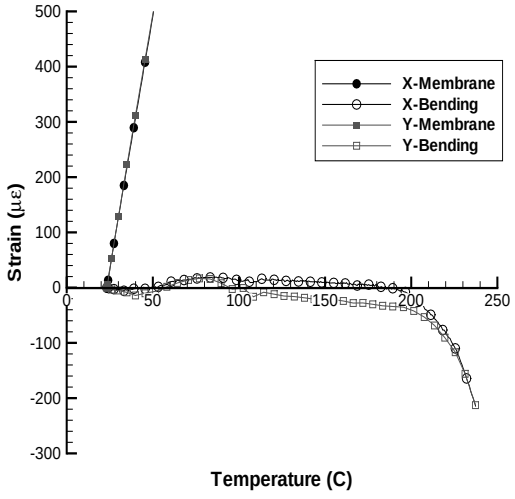

Figure 14: The strain history of the MFSP decomposed into bending and membrane strain

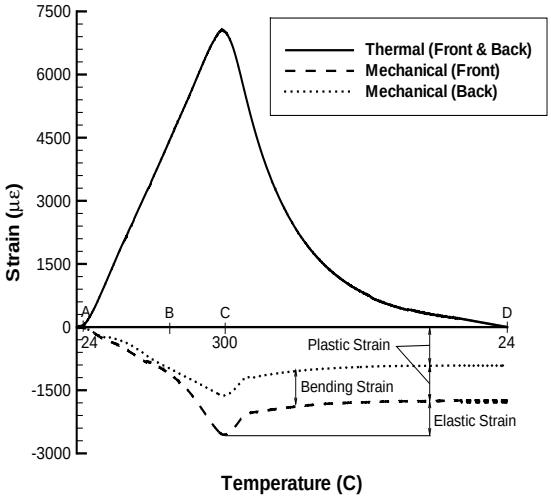

Figure 16: Thermal and mechanical strain throughout the loading cycle

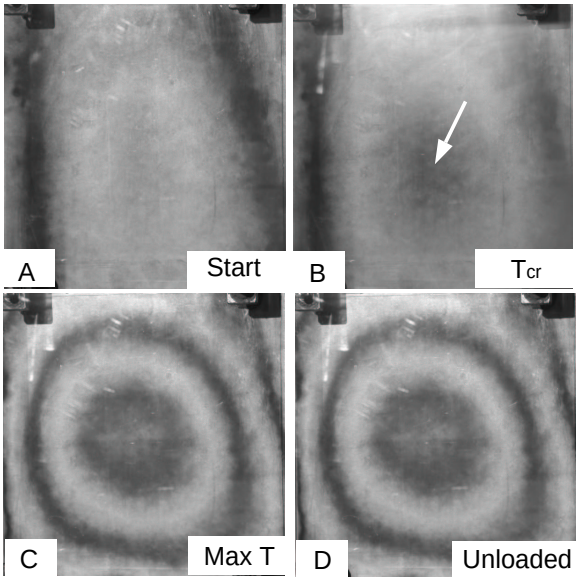

Figure 17: Digital images of the moire fringes which illustrate the full-field buckling modes on the surface of an MFSP. Each fringe represents $\Delta w = 0.264mm$ $(0.0104in)$.

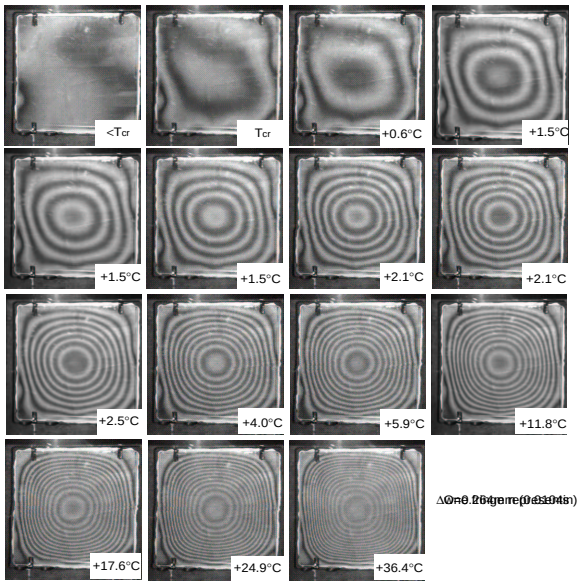

Figure 18: Digital images of the moire fringes which illustrate the full-field buckling modes on the surface of the imperfect MFSP. Each fringe represents $\Delta w = 0.264mm$ $(0.0104in)$.

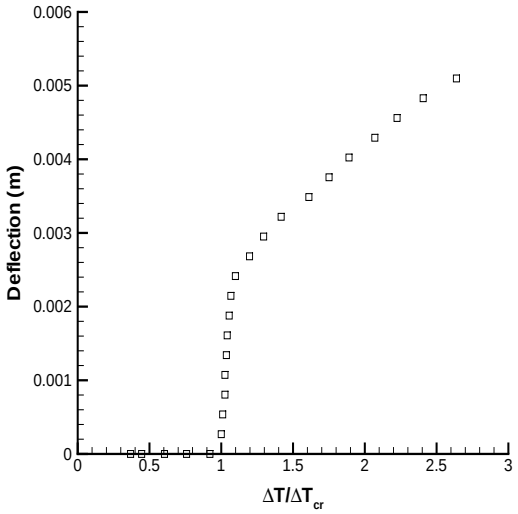

Figure 19: The amplitude of the buckled mode shape throughout the thermal response of the MFSP

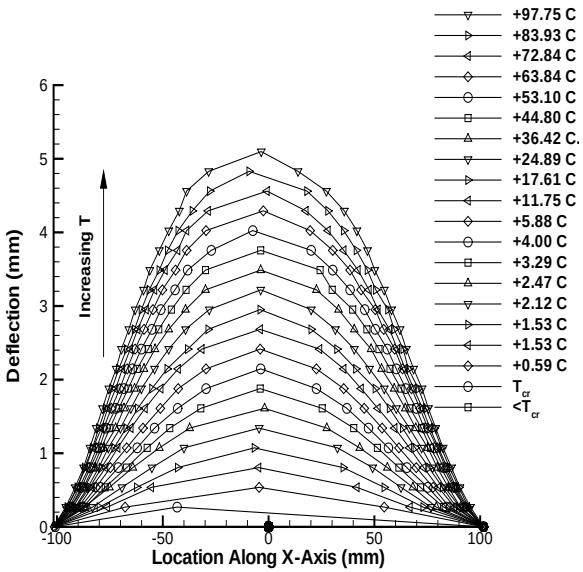

Figure 20: Response history of a line lying along the x-axis on the surface of the MFSP